Depth variance in the stoichiometry of marine organic matter respiration and the implications for the global oxygen cycle

Skylar D. Gerace[1], Adam J. Fagan[1], François W. Primeau[1], Allison R. Moreno[2,3], Paul Lethaby[4], Rodney J. Johnson[4], and Adam C. Martiny[1,2'*]

1. University of California, Irvine; Earth System Sciences. 3200 Croul Hall, Irvine, CA 92697, USA.
2. University of California, Irvine; Ecology and Evolutionary Biology. 321 Steinhaus Hall, Irvine, CA, 92697,USA
3. University of California, Los Angeles; Atmospheric and Oceanic Sciences. 520 Portola Plaza, Los Angeles, CA 90095, USA.
4. Bermuda Institute of Ocean Sciences. 25 Biological Station, St. George's GE 01, Bermuda.

*Corresponding author: amartiny@uci.edu

Highlights

- The respiration quotient varied with depth
- Elemental ratios of particulate organic matter deviated from Redfield proportions at all depths
- The increase in the respiration quotient with depth may account for some previously unexplained oxygen loss

Index Terms and Keywords

- 4805 Biogeochemical cycles, processes, and modeling; 4850 Marine organic chemistry; 4803 Analytical chemistry

Abstract

Climate warming is likely resulting in ocean deoxygenation, but models still cannot fully explain the observed decline in oxygen. One unconstrained parameter is the oxygen demand for respiring particulate organic carbon and nitrogen (i.e., the total respiration quotient, $r_{\Sigma\text{-}O2:C}$). It is untested if $r_{\Sigma\text{-}O2:C}$ systematically declines with depth. Here, we tested for such depth variance by quantifying particulate organic carbon (POC), particulate organic nitrogen (PON), particulate organic phosphorus (POP), particulate chemical oxygen demand (PCOD, the oxygen demand for respiring POC), and total oxygen demand ($-O_2$ = PCOD + 2PON) concentrations down to a depth of 1000 m in the Sargasso Sea. C:N and $-O_2$:N changed with depth, but values at the surface were similar to those at 1000 m. C:P, N:P, and $-O_2$:P exponentially decreased with depth. The respiration quotient ($r_{\text{-}O2:C}$ = PCOD:POC) and total respiration quotient ($r_{\Sigma\text{-}O2:C}$ = $-O_2$:POC) were both higher below the euphotic zone. We hypothesize that $r_{\Sigma\text{-}O2:C}$ is linked to multiple environmental factors that change with depth, such as phytoplankton community structure and the preferential production/removal of biomolecules. Using a global model, we show that the global distribution of dissolved oxygen is sensitive to changes in the PCOD surface production (P_{PCOD}) and depth attenuation (b_{PCOD}). These variables mostly affect oxygen in the tropical and North Pacific Ocean, where deoxygenation rates and model discrepancy are the highest. This study aims to improve our understanding of biological oxygen demand as warming-induced deoxygenation continues.

Plain Language Summary

Rising ocean temperatures are likely causing the observed decline of dissolved oxygen below the ocean surface. This continued oxygen loss threatens the survival of many marine animals. Currently, global models cannot fully explain the observed rate of oxygen loss with warming. One missing component could be variance in the respiration quotient, the ratio of oxygen consumed per organic carbon respired. However, the respiration quotient has yet to be estimated at different depths by directly measuring the chemical composition of organic matter. Here, we used direct measurements to find that the respiration quotient varied with depth in the western Atlantic Ocean. Therefore, the respiration quotient at the surface should not represent values at deeper depths. In addition, we used a global model to find that the respiration quotient mostly affects oxygen in the tropical and North Pacific Ocean, where unexplained oxygen loss is the highest. Therefore, more extensive data on the respiration quotient may significantly improve global models

1 Introduction

Climate warming is anticipated to lead to a reduction of dissolved oxygen in the ocean interior (Schmidtko et al., 2017; Levin, 2018). This deoxygenation will put many animal species at risk of extinction (Gallo & Levin, 2016; Breitburg et al., 2018), and significantly impact global carbon and nitrogen cycles (Keeling et al., 2010). The rate of ocean deoxygenation is calculated through models that incorporate established mechanisms by which ocean warming contributes to oxygen loss. Currently, it is known that warming decreases oxygen solubility, decreases the vertical transport of oxygen, and increases respiration rates (Shepherd et al., 2017). However, oxygen models can only capture ~50% of the observed deoxygenation rate (Oschlies et al., 2018), with the largest discrepancy in tropical thermocline waters (Stramma et al., 2012). It is hypothesized that this discrepancy will decrease with a better understanding of the stoichiometric demand for dissolved oxygen when respiring organic carbon and nitrogen (Robinson, 2019).

In the open ocean, the oxygen demand is controlled by elemental ratios of organic matter (Redfield, 1934; Anderson, 1995). First, from a mass balance approach, phytoplankton C:N and C:P link a limiting nutrient supply to the abundance of respirable compounds (Dugdale, 1967). Second, considering the reaction for respiring an organic compound:

(1) $$C_x(H_2O)_w(NH_3)_yH_zH_3PO_4 + (x + ¼\ z)O_2 \rightarrow xCO_2 + yNH_3 + H_3PO_4 + (w + ½\ z)H_2O$$

the oxygen demand for respiring organic carbon (i.e., the respiration quotient, $r_{\text{-}O2:C}$) is dependent on the carbon oxidation state (C_x:H_z in Equation 1; Paulmier et al., 2009). Therefore, $r_{\text{-}O2:C}$ is sensitive to proportions of biomolecules, since lipids are more chemically-reduced than carbohydrates (Laws, 1991). Third, due to additional oxygen consumption for nitrification:

(2) $$yNH_3 + (2y)O_2 \rightarrow yHNO_3 + yH_2O$$

the oxygen demand for respiring nitrogen is also dependent on C:N of organic matter (Babbin et al., 2014). Despite the effects of variable stoichiometry, a fixed C:N:P:-O_2 is still commonly prescribed in biogeochemical models (Robinson, 2019). Observations show that C:N:P:-O_2 varies between phytoplankton lineages (Finkel et al., 2016; Jónasdóttir, 2019), and is linked to temperature and nutrient stress (Liefer et al., 2019; Moreno et al., 2022). Variable C:N:P:-O_2 has

also been estimated from steady-state modeling (Takahashi et al., 1985; Anderson & Sarmiento, 1994) and bottle incubations (Arístegui et al., 2005) with mixed reviews and many caveats (Robinson, 2019). However, C:N:P:-O_2 has yet to be measured throughout the water column using direct elemental analysis of particulate organic matter (POM).

C:N:P:-O_2 of POM may vary with depth in the open ocean. Direct H:C measurements from sinking POM have shown decreasing trends with depth (Karl & Grabowski, 2017). This suggests an increase in the carbon oxidation state of POM through the water column and a possible decrease in $r_{\text{-}O2:C}$. The vertically-changing carbon oxidation state may result from the partial oxidation of sinking organic matter, or selective feeding by zooplankton for energy-rich (i.e., more chemically-reduced) food throughout the upper ocean (Karl & Grabowski, 2017; Gunina & Kuzyakov, 2022). Additionally, C:N of POM often increases with depth (Schneider et al., 2003), which has been attributed to the preferential recycling of nitrogen-rich compounds by bacterial decomposers (Olesen & Lundsgaard, 1995). We hypothesize that the total respiration quotient for respiring both carbon and nitrogen of POM ($r_{\Sigma\text{-}O2:C}$) systematically declines with depth due to these drivers of H:C and C:N.

Here, we test whether $r_{\Sigma\text{-}O2:C}$ decreases with depth by quantifying particulate organic carbon (POC), particulate organic nitrogen (PON), particulate organic phosphorus (POP), and particulate chemical oxygen demand (PCOD, the oxygen demand for respiring POC) concentrations from the surface to 1000 m deep. In addition, we use a steady-state model to determine the global dissolved oxygen sensitivity to $r_{\text{-}O2:C}$ variance. We also address how C:N:P:-O_2 compares to the Redfield (1934) proportions with depth, identify the environmental processes that likely drive depth variance in $r_{\Sigma\text{-}O2:C}$, and discuss how our results impact oxygen cycling in the interior ocean.

2 Methods

2.1 Cruise Stations

We sampled seawater and collected hydrographic data aboard the R/V *Atlantic Explorer* as part of the Bermuda Atlantic Times-series Study (BATS) Validation Cruise 58 (BVal58) (Figure 1). For BVal58, the cruise started at St. George's, Bermuda on 11 October 2021 and ended at San Juan, Puerto Rico on 21 October 2021. We sampled seawater and collected hydrographic data at a total of 13 stations (Stations #2 - 14) including the BATS site (Station #2). The 13 stations followed a transect from 31°40'N 64°10'W to 19°40'N 65°58'W separated by 1° in latitude. Seawater sampling and hydrographic data collection occurred at random times

throughout the 24 h cycle. We measured elemental concentrations of POM throughout the euphotic zone (5 - 120 m) at all 13 stations, and throughout the disphotic zone (150 - 1000 m) at 5 stations (Stations #2, 5, 9, 11, & 12).

2.2 Hydrography

Temperature, dissolved oxygen concentration, and chlorophyll-a fluorescence were measured using a Sea-bird 911 CTD at all 13 stations. These variables were quantified at depths of 5 - 1000 m, with depth binned as every 2 m. For each station, the depth below the mixed layer where chlorophyll-a fluorescence intensity reached a maximum was the depth of the deep chlorophyll maximum (DCM). The DCM depth can be used to estimate the base of the euphotic zone (Terzić et al., 2019), and proxy the nutricline depth, an indicator of surface nutrient scarcity (Estrada et al., 1993).

2.3 Nutrient Sampling

Nitrate and phosphate concentrations were measured from all sampled depths. Seawater for nutrient determination was sampled using a JGOFS protocol by Ducklow & Dickson (1994) and updated by Sanderson et al. (1997). The seawater was filtered by attaching an 0.8 μm Nuclepore filter to the spigot of an Ocean Test Equipment (OTE) bottle. The seawater was then bottled (HDPE) and frozen at -20 ^{o}C until analysis. Nitrate and phosphate were photometrically determined using Continuous Flow Analysis on a Technicon AutoAnalyzer II. To detect nitrate, the nitrate is first reduced to nitrite using a copperized cadmium column. The nitrite reacts with 0.06 M sulfanilamide and then 4 mM N-(1-naphthyl)ethylene-1,2-diamine (NEDA) to produce a red azo dye. To detect phosphate, 0.186 M molybdic acid in 6.3 M sulfuric acid is introduced to phosphate to form a blue phosphomolybdenum solution.

2.4 POM Sampling in the Euphotic Zone (Depths of 5 - 120 m)

Seawater was collected in the euphotic zone at Stations #2 - 14 for determining elemental concentrations of POM (POC/N, POP, & PCOD). At Station #2 and #9, we sampled POM 4 and 3 times respectively to constrain any diel variation. A total of 18 casts were made in the euphotic zone. Per cast, seawater was collected at 5, 40, 80, and 120 m deep using a CTD rosette fitted with twenty-four 10 L Niskin bottles (OTE). All sampling carboys were rinsed 3 times with collected seawater before filling to 8 L. POM was collected on 25 mm GF/F filters (0.7 μm pore size, Whatman, GE Healthcare) pre-combusted at 500 °C for 4 h. The 6 filters collected at each depth of each station resulted in duplicate samples for the POC/N, POP, and

PCOD assays. After filtering 8 L, the filters for the POP assay were rinsed with 5 mL of 0.17 M $NaSO_4$ to remove dissolved inorganic phosphorus, and the filters for the PCOD assay were rinsed with 5 mL of deionized water to remove chloride ions. All filters were folded in half after filtration, sealed inside pre-combusted aluminum foil (500˚C for 4 h), and stored at -80 °C. Post-assays, we accounted for POM on blank filters by subtracting the average value of 10 dry blanks. The dry blanks were pre-combusted filters that had not been used for filtering.

2.5 POM Sampling in the Disphotic Zone (Depths of 150 - 1000 m)

The methodology for sampling seawater in the disphotic zone was different due to the low POM concentrations. We deployed McLane Large Volume - Water Transfer System (WTS-LV) pumps at 5 stations (Stations #2, 5, 9, 11, & 12) to filter large volumes of seawater. Per cast, McLane pumps were lowered to depths of 150, 200, 300, 400, 500, and 1000 m. Each McLane pump directly filtered 557 - 821 L of seawater through a 142 mm diameter pre-combusted GF/F filter (0.7 µm pore size, Whatman, GE Healthcare). After recovering the McLane pumps, the filters were similarly folded in half, sealed with pre-combusted aluminum foil, and stored at -80 °C.

On shore, we hole-punched the 142 mm diameter filters in 15 places with a carbon-steel 18 mm hole-puncher that had been pre-combusted (500 °C for 4 h). Since the filters were still folded in half, each hole-punch created a pair of chads that were stuck together with organic matter in between them, resembling an “Oreo cookie.” These chad pairs had a diameter of 18 mm and were a sufficient size for the assays. Taking into account the O-ring, two 18 mm diameter circles equal 3.8% of the total filter area containing POM. 1 - 4 chad pairs served as one replicate sample depending on the sensitivity of the assay. 2 - 4 replicate samples were made for each assay. Dry blanks were prepared by hole-punching a pre-combusted, but unused 142 mm GF/F filter.

2.6 Particulate Organic Carbon and Nitrogen (POC/N) Assay

Particulate organic carbon and nitrogen were quantified from the same filter. The POC/N samples were processed using a JGOFS protocol (Ducklow & Dickson, 1994). Filters for the POC/N assay were dried at 55 °C for 24 h. Filters were then placed in a desiccator with 12 M hydrochloric acid for 24 h to remove inorganic carbonates. Filters were then re-dried for a minimum of 48 h at 55 °C. After drying, the filters were folded and pelletized into pre-combusted tin capsules (CE Elantech, Lakewood, NJ). Each tin-wrapped sample was analyzed in a FlashEA 1112 Elemental Analyzer using the NC Soils setup (Thermo Scientific, Waltham, MA).

Known masses of atropine and acetanilide were used as standards for each run. The minimum detection limits for carbon and nitrogen were 2.4 µg and 3.0 µg respectively.

2.7 Particulate Organic Phosphorus (POP) Assay

We quantified particulate organic phosphorus using an ash-hydrolysis method presented by Lomas et al. (2010). Filters were placed in autoclaved glass vials with 2 mL of 0.017 M $MgSO_4$, covered with pre-combusted aluminum foil (500 ^oC for 4 h), and then combusted at 500 ^oC for 2 h. 5 mL 0.2 M HCl was added and incubated at 80 - 90 ^oC for 30 min. After cooling, the solution was poured into a glass centrifuge tube. The glass vial was rinsed with 5 mL of deionized water, which was then poured into the same centrifuge tube. A mixed reagent of 0.0243 M ammonium molybdate tetrahydrate, 5 N sulfuric acid, 0.004 M potassium antimonyl tartrate, and 0.3 M ascorbic acid (2:5:1:2) was added to each tube before being set in the dark for 30 min. Tubes were then centrifuged at 4000 rpm and quantified at 885 nm with a spectrophotometer using a potassium monobasic phosphate standard (1.0 mM-P).

2.8 Particulate Chemical Oxygen Demand (PCOD) Assay

The PCOD assay is a wastewater assay that has been modified by Moreno et al. (2020) to accurately quantify oxygen needed to fully oxidize organic carbon on GF/F filters. Note that because dichromate does not oxidize ammonium, this assay does not quantify oxygen demand for nitrification. Prior to the assay, the filters were dried at 55 °C for at least 24 h. For analysis, filters were added into HACH COD HR+ reagent vials (Product no. 2415915 containing mercuric sulfate) with 2 mL of milli-Q water. Vials were digested at 150 °C for 2 h, then 92.1 µL of 0.163 M NaCl was added to induce even precipitation of silver chloride. Vials were then inverted twice and centrifuged for 30 min at 2,500 rpm. The absorbance of each vial was measured at 600 nm using a spectrophotometer. The oxygen demand was quantified using a standard curve made from HACH certified phthalate-based standards.

2.9 Calculating Ratios and $-O_2$

Elemental ratios (µM:µM) were quantified using mean concentrations from the same depth and station. Here, the respiration quotient ($r_{-O2:C}$) is defined as ratio of PCOD to POC. We quantified the total oxygen demand for respiring both organic carbon and nitrogen ($-O_2$) as PCOD plus double PON in units of micromolar (Equations 1 and 2; Paulmier et al., 2009). The total respiration quotient ($r_{\Sigma-O2:C}$) is the ratio of $-O_2$ to POC.

2.10 Depth Variance in Ratios with Respect to Redfield Proportions

We defined X* for all elemental ratios similarly to how Gruber & Sarmiento (1997) defined the nutrient tracer N*. Considering a ratio's numerator (*n*), denominator (*d*), and respective Redfield proportion value (*R*):

$$X* = n - (d \times R) \quad (3)$$

R was 106/16, 106/1, and 16/1 for C:N, C:P, and N:P respectively. *R* was 1.0 and 1.3 for $r_{\text{-}O2:C}$ and $r_{\Sigma\text{-}O2:C}$ (Redfield, 1934). We refer to X* of a ratio based on the ratio's numerator and denominator (e.g., the X* of C:N is called CN*).

2.11 Statistical Tests and Regression Models

First, we tested for latitudinal and temporal variability in the elemental concentrations from the euphotic zone. We evaluated each elemental concentration as a linear combination of depth and latitude. Second, we defined each concentration from the euphotic zone as another linear combination using depth and the local time when seawater was sampled. In this model, we incorporated the time of day as part of a sinusoidal function that indicates the intensity of sunlight at the sampling hour (Garcia et al., 2022). Elemental concentrations (*y*), depth (*D*), and sampling hour (*t*) were defined such that:

$$y = c_c + c_D(D) + A\,sin(\pi t/12 + \phi) \quad (4)$$

Lastly, we tested the hypothesis that the $r_{\Sigma\text{-}O2:C}$ systematically decreased with depth by defining $r_{\Sigma\text{-}O2:C}$ as a linear function of depth. Models were considered to be significant if an F-test determined that all coefficients were significant ($p > 0.05$).

2.12 The Sensitivity of Global Dissolved Oxygen to $r_{\text{-}O2:C}$ Variance

It is uncertain how variance in $r_{\text{-}O2:C}$ impacts the global dissolved oxygen distribution. Building on the model of Wang et al. (2019), Moreno et al. (2020) created a steady-state model to predict this distribution based on the surface production and depth attenuation of PCOD and POC fluxes. In the model, $r_{\text{-}O2:C}$ varies at the surface as a function of sea surface temperature. The production rate of PCOD (P_{PCOD}) is defined as POC production multiplied by $r_{\text{-}O2:C}$. The depth attenuation of PCOD follows a Martin curve with a characteristic *b*-exponent (b_{PCOD}) (Martin et al., 1987). P_{PCOD} and b_{PCOD} are adjustable model variables whose values and

associated uncertainties are estimated using hydrographic dissolved oxygen and dissolved inorganic carbon distributions. Using this approach of Moreno et al. (2020), we predicted the global distribution of dissolved oxygen at a depth of 1000 m under four scenarios: 90% P_{PCOD}, 110% P_{PCOD}, 90% b_{PCOD}, and 110% b_{PCOD}. For each scenario, we compared the predicted oxygen distribution to the observed distribution at a global scale.

3 Results

To test our hypothesis, we quantified hydrographic data and POM elemental concentrations in the western North Atlantic Ocean (Figure 1). POC, PON, POP, and PCOD concentrations were quantified throughout the euphotic zone (5 - 120 m) at 13 stations, and the disphotic zone (150 - 1000 m) at 5 stations. POM ratios (C:N, C:P, and N:P) and respiration ratios ($r_{\text{-}O2:C}$, $r_{\Sigma\text{-}O2:C}$, -O_2:N, and -O_2:P) were quantified using mean concentrations from unique depths and stations. In addition, we used a steady-state model (Moreno et al., 2020) to determine the sensitivity of global oxygen at 1000 m depth to $r_{\text{-}O2:C}$ variance. We varied $r_{\text{-}O2:C}$ by changing either PCOD surface production (P_{PCOD}) or depth attenuation (b_{PCOD}) by ±10%. Here, we first describe the hydrographic setting of our observations, then present the observed variability in elemental concentrations and ratios, and lastly report the modeled sensitivity of global oxygen to $r_{\text{-}O2:C}$ variance.

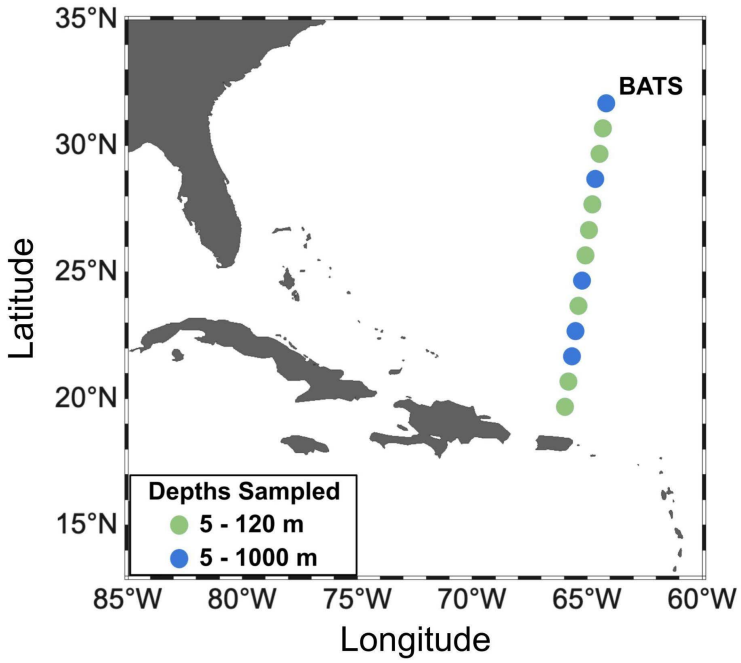

Figure 1: Map of station from BATS validation cruise. Stations #2 - 14 of the Bermuda Atlantic Time-series Study Validation cruise #58 (31°40'N 64°10'W to 19°40'N 65°58'W). The cruise went from St. George's, Bermuda to San Juan, Puerto Rico, 11-21 October 2021. Station #2 is the site of the Bermuda Atlantic Time-series Study (BATS). We measured concentrations of POM in the euphotic zone (5, 40, 80, & 120 m depth) at all 13 stations, and in the disphotic zone (150, 200, 300, 400, 500, & 1000 m depth) at Stations #2, 5, 9, 11, & 12.

3.1. Hydrography

We observed clear vertical gradients and limited latitudinal gradients in hydrographic conditions (Figure S1 in Supporting Information S1). Sea surface temperature steadily increased from north to south by ~3˚C. Temperature in the disphotic zone was relatively constant throughout the transect, except for slightly higher temperatures below 300 m at 19 - 21°N. Dissolved oxygen concentrations declined from north to south in both the euphotic and disphotic zones. The highest concentrations of dissolved oxygen were towards the base of the euphotic zone at 27 - 32°N, whereas a concentration minimum was seen at 400 - 900 m from 20 - 24°N. Chlorophyll-a fluorescence reached maximum values at depths of 100 - 130 m, defining the deep chlorophyll maximum and approximate upper bound of the euphotic zone base. The nutricline depth (where nitrate reaches 1 µmol/kg) ranged from 150 - 200 m depth. Considering the limited latitudinal gradient in hydrographic conditions, we expected to find limited latitudinal variability in the elemental concentrations and ratios.

306
307 **3.2 Latitudinal and Temporal Variability of Elemental Concentrations**
308 Elemental concentrations from the euphotic zone did not have strong latitudinal or
309 temporal variability (Figure S2 in Supporting Information S1). We tested for significant latitudinal
310 variability by defining each concentration in the euphotic zone as a linear combination of depth
311 and latitude. Only POC varied with latitude (Table S1 in Supporting Information S1). We also
312 tested if concentrations in the euphotic zone showed diel shifts, but only PCOD showed any
313 significant changes with time (±0.8 μM) and peaked toward the end of the photic period (5:20
314 pm; Figure S3 and Table S2 in Supporting Information S1). Since elemental concentrations from
315 the euphotic zone showed limited latitudinal and diel variability, we treated all casts as replicates
316 for determining the depth variance in ratios.
317
318 **3.3 Elemental Concentrations and Ratios vs. Depth**
319 We found clear depth variance in elemental concentrations and ratios (Figure 2). The
320 highest mean concentrations of PCOD and POC were detected at the surface, whereas PON
321 and POP peaked at 80 m (Figure 2a). All elemental concentrations exponentially decreased
322 with depth below 80 m (Figure 2a). C:N and $-O_2$:N generally decreased from the surface to 500
323 m, but increased back to surface values at 1000 m (Figures 2b and 2c). In contrast, C:P, N:P,
324 and $-O_2$:P consistently decreased from the surface to 1000 m (Figures 2b and 2c). $r_{-O2:C}$ and $r_{\Sigma-O2:C}$
325 decreased with depth in the euphotic zone, but increased in the disphotic zone (Figure 2c).
326 There was a large change in most ratios from 120 m to 150 m, which may be in part due to the
327 different sampling methods (Figures 2b and 2c). When defining $r_{\Sigma-O2:C}$ as a linear function of
328 depth from the surface to 1000 m, $r_{\Sigma-O2:C}$ increased with depth (slope [SE] = 3.0×10^{-4} [6.2×10^{-5}],
329 intercept [SE] = 1.3 [0.02], $p = 7 \times 10^{-6}$). Generally, PCOD and PON declined more slowly
330 with depth than POC and POP, and some ratios exhibited a change in trend below the euphotic
331 zone.
332
333

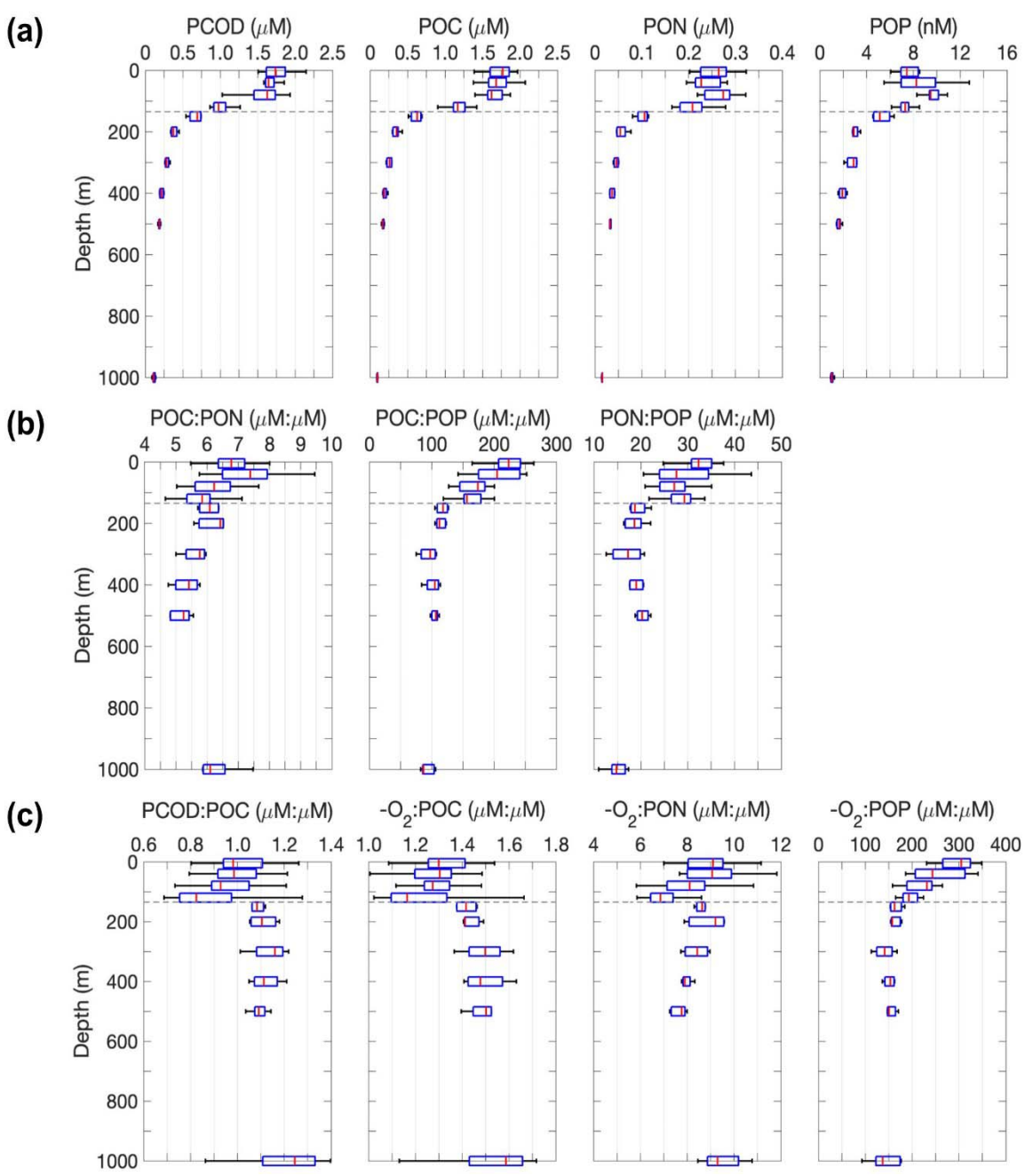

Figure 2: Depth profiles of elemental concentrations and ratios. (a) Elemental concentrations, (b) POM ratios, and (c) respiration ratios were quantified at depths of 5, 40, 80, 120, 150, 200, 300, 400, 500, and 1000 m (N = 19, 16, 17, 17, 4, 5, 4, 4, 5, and 5 respectively). $-O_2$ = PCOD + 2PON in units of micromolar. $r_{-O2:C}$ is PCOD:POC and $r_{\Sigma-O2:C}$ is $-O_2$:POC. The gray dashed line separates the euphotic and disphotic zones, which had been sampled using different methods (see Methods). Red lines show the medians, blue boxes show the 25th and 75th percentiles, and black whiskers show the 5th and 95th percentiles.

3.4 Depth Variance in Ratios with Respect to Redfield Proportions

The elemental ratio tracer (X*) showed that all ratios deviated from Redfield (1934) proportions at some depths (Figure 3). C:N, C:P, and -O_2:N were greater than Redfield proportions in the upper euphotic zone, but fell below in the disphotic zone. N:P and -O_2:P were elevated from Redfield proportions at 500 m and above, but nearly matched at 1000 m. $r_{\text{-O2:C}}$ and $r_{\Sigma\text{-O2:C}}$ were less than Redfield proportions in the euphotic zone, but rose above in the disphotic zone. In conclusion, the oxygen demand below the euphotic zone is generally greater than expected from C or P, but less than from N.

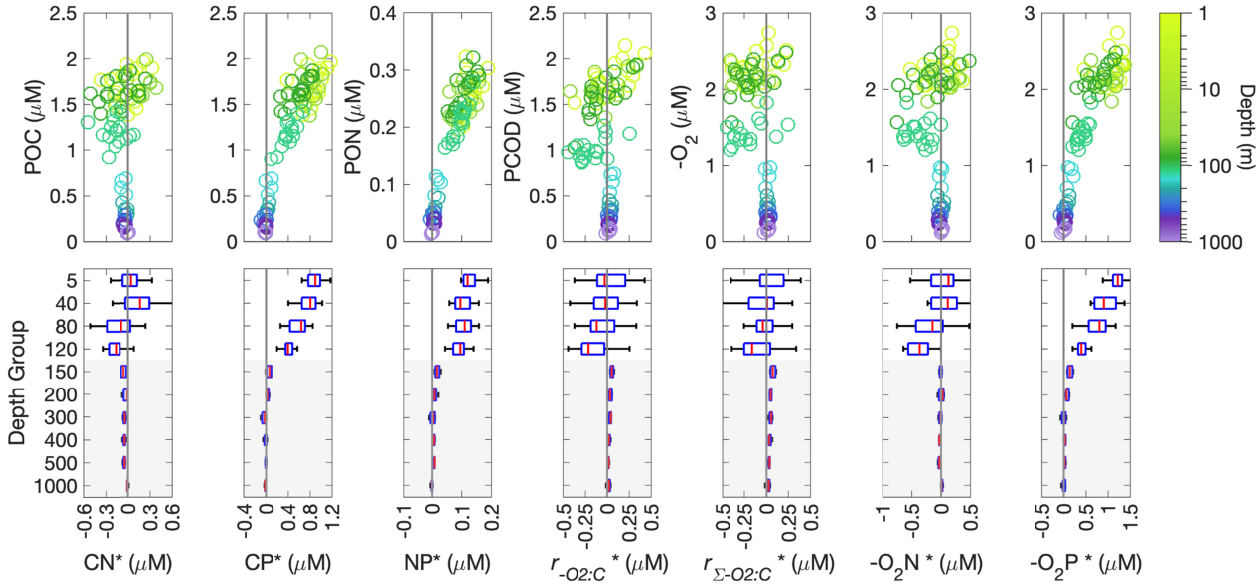

Figure 3: Depth profiles of elemental anomalies. X* the POM ratios (C:N, C:P, & N:P) and respiration ratios ($r_{\text{-O2:C}}$, $r_{\Sigma\text{-O2:C}}$, -O_2:N, & -O_2:P) with respect to the proportions suggested by Redfield (1934) (i.e., C:N:P:-O_2 = 106:16:1:138). Redfield (1934) suggests that $r_{\text{-O2:C}}$ = 1.0 and $r_{\Sigma\text{-O2:C}}$ = 1.3. The scatter plots are the X* vs. the ratio numerator (*n*) from Equation 3. The value of X* = 0 is where a ratio is equal to Redfield proportions. For the box plots, the groups are named after the depth in meters where samples were collected. Different methods were used to sample the euphotic zone (unshaded) and disphotic zone (shaded) groups (See Methods). Red lines show the medians, blue boxes show the 25th and 75th percentiles, and the black whiskers show the 5th and 95th percentiles.

3.5 The Sensitivity of Global Dissolved Oxygen to $r_{-O2:C}$ Variance

In the steady-state model by Moreno et al. (2020), changing the PCOD surface production (P_{PCOD}) vs. depth attenuation (b_{PCOD}) had different regional impacts on the global distribution of dissolved oxygen (Figure 4). Our observed PCOD and POC concentrations at 1000 m were one order of magnitude higher than the global averages estimated by the model (Figures 4a and 4b). $r_{-O2:C}$ at 1000 m was more sensitive to a 10% change in b_{PCOD} rather than P_{PCOD} (Figures 4a and 4b). Changing P_{PCOD} or b_{PCOD} resulted in similar distributions of oxygen sensitivity, with the highest sensitivity occurring in the tropical and North Pacific Ocean (Figure 4c). Between the two variables, b_{PCOD} had a stronger effect in this region, especially in the California Current System (Figure 4c). In contrast, P_{PCOD} had greater influence over the Atlantic Ocean, Arctic Ocean, and Arabian Sea (Figure 4c). When comparing opposite scenarios of the same variable, a 10% increase had an almost identical distribution as a 10% decrease for both P_{PCOD} and b_{PCOD} (Figure S4 in Supporting Information S1). In addition, the total O_2 at 1000 m was equally sensitive to a 10% change in P_{PCOD} or b_{PCOD} (Figure 4c). In summary, changing P_{PCOD} or b_{PCOD} resulted in similar distributions of oxygen sensitivity at 1000 m, but b_{PCOD} had a greater effect on oxygen in the North Pacific.

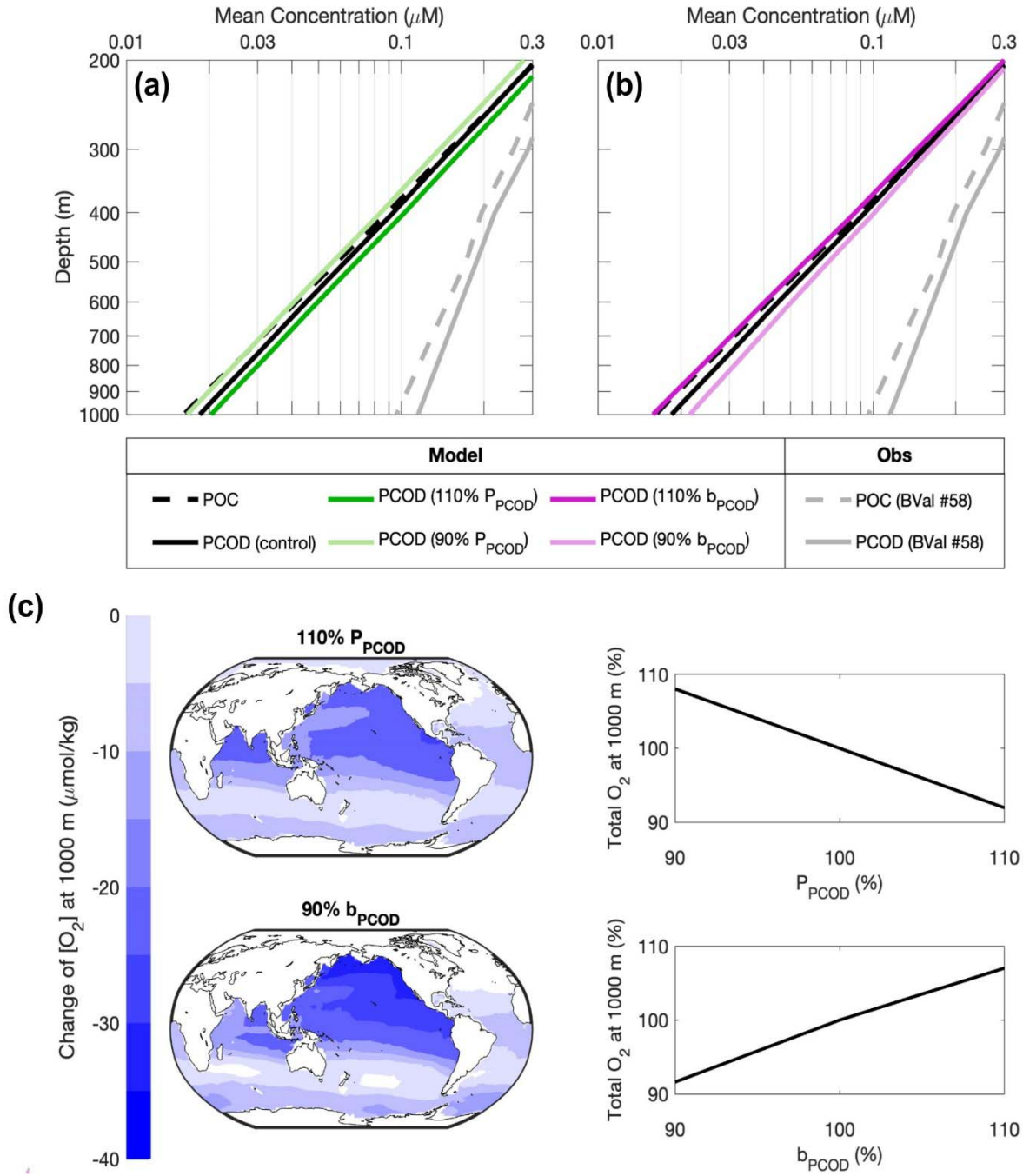

Figure 4: Sensitivity of global ocean oxygen to variation in the respiration quotient. (a,b) Depth profiles of PCOD and POC from the model scenarios and observations. Modeled concentrations originate from globally-averaged predictions based on hydrographic dissolved oxygen and dissolved inorganic carbon distributions. Observed concentrations are averaged from the BVal58 data set. (c) the sensitivity of global oxygen at 1000 m deep to ±10% b_{PCOD} (depth attenuation) or P_{PCOD} (production).

4 Discussion

We did not find evidence that the $r_{\Sigma\text{-}O2:C}$ vertically declines from the surface to 1000 m and thus reject our initial hypothesis. $r_{\Sigma\text{-}O2:C}$ did decline with depth in the euphotic zone, which is possibly due to changes in phytoplankton physiology rather than the removal processes suggested in Karl & Grabowski (2017). For example, phytoplankton at deeper depths have larger cell size, thus a lower percentage of biomass is attributed to their phospholipid membrane (Arin et al., 2002; Latasa et al., 2016). Lower light intensity at the base of the euphotic zone also decreases lipid over carbohydrate production by phytoplankton (Suárez & Marañón, 2003; Rayati et al., 2020). However, the select removal of more oxidized biomolecules, such as carbohydrates, could be driving the elevated $r_{\Sigma\text{-}O2:C}$ observed in the disphotic zone (Liu et al., 2022). In addition, some chemically-reduced carbon that sinks may be preserved from bacterial degradation and accumulate in the disphotic zone (Lee et al., 2004). Therefore, a higher abundance of more reduced carbon may explain a higher $-O_2$:N found in the Sargasso Sea, rather than underestimated C:N (Fawcett et al., 2018). To conclude, $r_{\Sigma\text{-}O2:C}$ varies with depth, thus surface values alone should not be used to constrain oxygen consumption at deeper depths.

C:N:P with depth may explain some nuances in the respiration ratios. Here, the trend of C:N with depth is similar to Hansell & Carlson (2001), which may be due to increasing bacterial abundance with depth (Gunderson et al., 2002). However, global POM trends show increasing C:N and C:P with depth in most regions (Schneider et al., 2003; Tanioka et al., 2021). Higher C:N and C:P with depth result in a higher $-O_2$:N and $-O_2$:P than what is estimated from nutrient flux alone (DeVries & Deutsch, 2014). In addition, N:P is considered to generally increase due to the faster attenuation of P, however we found that N:P decreased with depth (Clark et al., 1998). Nevertheless, our measurements of elevated N:P show that the euphotic zone $r_{\text{-}O2:C}$ is depressed under P limitation (Geider & La Roche, 2002; Klausmeier et al., 2004). Similarly, Moreno et al. (2022) found that the surface $r_{\text{-}O2:C}$ is depressed in P stressed regions of the eastern Pacific and Atlantic oceans. In summary, C:N:P relates respiration ratios to nutrient flux and the type of nutrient stress present.

Here we present the first data set of C:N:P:$-O_2$ measured at different depths by direct elemental analysis of POM, but there are multiple caveats to our results. First, POM concentrations measured from large volume pumps were on average lower than concentrations from Niskin bottles at the same depths (Figure S5 in Supporting Information S1). This is consistent with past observations showing that large volume pumps can lead to lower estimates of POM elemental concentrations (Altabet et al., 1992; Schneider et al., 2003). In addition, the

lower deviation between concentrations from the disphotic zone is in part due to the lower sampling size. This difference in sampling technique can also contribute to some of the variance in elemental ratios at the bottom of the euphotic zone, but will not affect the gradients within either the euphotic or disphotic zones. Despite a potential bias between our two sampling methods, our elemental concentrations still fall within expected ranges with respect to depth, region, and season (Lomas et al., 2010; Lomas & Moran, 2011). Second, the Sargasso Sea has a unique ecosystem due to the high production of the *Sargassum* macroalgae (Stoner & Greening, 1984). The trends we found in the ratios may be due to regional drivers distinct from the global ocean. Thus, measurements of vertical C:N:P:-O_2 gradients in other regions are needed. Third, we do not know the proportion of the POM respired at each depth since we measured standing stocks rather than sinking rates (Shanks & Trent, 1980; Buesseler et al., 2020). This uncertainty makes it harder to constrain the true oxygen demand at each depth. It is important to recognize these limitations if incorporating the observed stoichiometric gradients into global models.

Despite these caveats, we introduce observational data describing $r_{\text{-}O2:C}$ and $r_{\Sigma\text{-}O2:C}$ depth variances, which are important for modeling global oxygen consumption. We observed PCOD and POC concentrations that are higher than the global averages estimated by the steady-state model, which is unexpected for the Sargasso Sea (Figures 4a and 4b) (Ono et al., 2001). However, the depth attenuation of POM could be overestimated by the model (Buesseler et al., 2020)**.** Nonetheless, P_{PCOD} and b_{PCOD} mostly affect oxygen in the tropical and North Pacific Ocean, where deoxygenation rates and model discrepancy are the highest (Stramma et al., 2012; Schmidtko et al., 2017). (Figure 4c). Model discrepancy of oxygen is thought to be mostly caused by unconstrained circulation, but $r_{\text{-}O2:C}$ spatial variance may explain some of the observed oxygen decline (Stramma et al., 2012). $r_{\text{-}O2:C}$ spatial variance is also subject to change, since POM depth attenuation and $r_{\text{-}O2:C}$ at the ocean surface are both hypothesized to increase with warming (Boscolo-Galazzo et al., 2018; Moreno et al., 2020). Additionally, increasing nutrient stress could increase C:N and C:P, which will affect estimating P_{PCOD} from nutrients (Bopp et al., 2001; Klausmeier et al., 2004). Hence, it is crucial to gather more observational data on C:N:P:-O_2 across various depths, regions, and seasons to enhance our understanding of whether the oxygen demand for respiration plays a role in the escalating rate of global deoxygenation.

Acknowledgments

We thank the captain and crew of the R/V *Atlantic Explorer* for implementing a safe and productive cruise. We thank the chief scientist, marine technicians, and other scientists aboard for their assistance in sampling. We thank the staff of the Bermuda Institute of Ocean Sciences for providing quarantine accommodations and service during the COVID-19 pandemic. This study was funded by the National Science Foundation (OCE-1948842 to ACM and FP).

Conflict of Interest

The authors declare no conflicts of interest relevant to this study.

Data Availability Statement

Data of the elemental concentrations and ratios are provided as Data Set S1. Hydrographic data for the BVal58 cruise are available from the BATS Data site (https://bats.bios.edu/bats-data/).

References

Altabet, M. A., Bishop, J. K. B., & McCarthy, J. J. (1992). Differences in particulate nitrogen concentration and isotopic composition for samples collected by bottles and large-volume pumps in Gulf Stream warm-core rings and the Sargasso Sea. *Deep Sea Research Part A. Oceanographic Research Papers*, *39*, S405–S417. https://doi.org/10.1016/S0198-0149(11)80022-1

Anderson, L. A. (1995). On the hydrogen and oxygen content of marine phytoplankton. *Deep Sea Research Part I: Oceanographic Research Papers*, *42*(9), 1675–1680. https://doi.org/10.1016/0967-0637(95)00072-E

Anderson, L. A., & Sarmiento, J. L. (1994). Redfield ratios of remineralization determined by nutrient data analysis. *Global Biogeochemical Cycles*, *8*(1), 65–80. https://doi.org/10.1029/93GB03318

Arin, L., Morán, X. A., & Estrada, M. (2002). Phytoplankton size distribution and growth rates in the Alboran Sea (SW Mediterranean): Short term variability related to mesoscale hydrodynamics. *Journal of Plankton Research*, *24*. https://doi.org/10.1093/plankt/24.10.1019

Arístegui, J., Duarte, C. M., Gasol, J. M., & Alonso-Sáez, L. (2005). Active mesopelagic prokaryotes support high respiration in the subtropical northeast Atlantic Ocean. *Geophysical Research Letters*, *32*(3). https://doi.org/10.1029/2004GL021863

Babbin, A. R., Keil, R. G., Devol, A. H., & Ward, B. B. (2014). Organic Matter Stoichiometry, Flux, and Oxygen Control Nitrogen Loss in the Ocean. *Science*, *344*(6182), 406–408. https://doi.org/10.1126/science.1248364

Bopp, L., Monfray, P., Aumont, O., Dufresne, J.-L., Le Treut, H., Madec, G., et al. (2001). Potential impact of climate change on marine export production. *Global Biogeochemical Cycles*, *15*(1), 81–99. https://doi.org/10.1029/1999GB001256

Boscolo-Galazzo, F., Crichton, K. A., Barker, S., & Pearson, P. N. (2018). Temperature dependency of metabolic rates in the upper ocean: A positive feedback to global climate change? *Global and Planetary Change*, *170*, 201–212. https://doi.org/10.1016/j.gloplacha.2018.08.017

Breitburg, D., Levin, L. A., Oschlies, A., Grégoire, M., Chavez, F. P., Conley, D. J., et al. (2018). Declining oxygen in the global ocean and coastal waters. *Science*, *359*(6371), eaam7240. https://doi.org/10.1126/science.aam7240

Buesseler, K. O., Boyd, P. W., Black, E. E., & Siegel, D. A. (2020). Metrics that matter for assessing the ocean biological carbon pump. *Proceedings of the National Academy of Sciences*, *117*(18), 9679–9687. https://doi.org/10.1073/pnas.1918114117

Clark, L. L., Ingall, E. D., & Benner, R. (1998). Marine phosphorus is selectively remineralized. *Nature*, *393*(6684), Article 6684. https://doi.org/10.1038/30881

DeVries, T., & Deutsch, C. (2014). Large-scale variations in the stoichiometry of marine organic matter respiration. *Nature Geoscience*, *7*(12), Article 12. https://doi.org/10.1038/ngeo2300

Ducklow, H. & Dickson, A. (1994). Chapter 2: Shipboard Sampling procedures. *JGOFS Protocols* (pp. 1-210).

Dugdale, R. C. (1967). Nutrient Limitation in the Sea: Dynamics, Identification, and Significance. *Limnology and Oceanography*, *12*(4), 685–695. https://doi.org/10.4319/lo.1967.12.4.0685

Estrada, M., Marrasé, C., Latasa, M., Berdalet, E., Delgado, M., & Riera, T. (1993). Variability of deep chlorophyll maximum characteristics in the Northwestern Mediterranean. *Marine Ecology Progress Series*, *92*, 289–300. https://doi.org/10.3354/meps092289

Fawcett, S. E., Johnson, K. S., Riser, S. C., Van Oostende, N., & Sigman, D. M. (2018). Low-nutrient organic matter in the Sargasso Sea thermocline: A hypothesis for its role, identity, and carbon cycle implications. *Marine Chemistry*, *207*, 108–123. https://doi.org/10.1016/j.marchem.2018.10.008

Finkel, Z. V., Follows, M. J., Liefer, J. D., Brown, C. M., Benner, I., & Irwin, A. J. (2016). Phylogenetic Diversity in the Macromolecular Composition of Microalgae. *PLOS ONE*, *11*(5), e0155977. https://doi.org/10.1371/journal.pone.0155977

Gallo, N. D., & Levin, L. A. (2016). Chapter Three—Fish Ecology and Evolution in the World's Oxygen Minimum Zones and Implications of Ocean Deoxygenation. In B. E. Curry

(Ed.), *Advances in Marine Biology* (Vol. 74, pp. 117–198). Academic Press. https://doi.org/10.1016/bs.amb.2016.04.001

Garcia, N. S., Talmy, D., Fu, W.-W., Larkin, A. A., Lee, J., & Martiny, A. C. (2022). The Diel Cycle of Surface Ocean Elemental Stoichiometry has Implications for Ocean Productivity. *Global Biogeochemical Cycles*, *36*(3), e2021GB007092. https://doi.org/10.1029/2021GB007092

Geider, R., & La Roche, J. (2002). Redfield revisited: Variability of C:N:P in marine microalgae and its biochemical basis. *European Journal of Phycology*, *37*(1), 1–17. https://doi.org/10.1017/S0967026201003456

Gruber, N., & Sarmiento, J. L. (1997). Global patterns of marine nitrogen fixation and denitrification. *Global Biogeochemical Cycles*, *11*(2), 235–266. https://doi.org/10.1029/97GB00077

Gundersen, K., Heldal, M., Norland, S., Purdie, D. A., & Knap, A. H. (2002). Elemental C, N, and P cell content of individual bacteria collected at the Bermuda Atlantic Time-series Study (BATS) site. *Limnology and Oceanography*, *47*(5), 1525–1530. https://doi.org/10.4319/lo.2002.47.5.1525

Gunina, A., & Kuzyakov, Y. (2022). From energy to (soil organic) matter. *Global Change Biology*, *28*(7), 2169–2182. https://doi.org/10.1111/gcb.16071

Hansell, D. A., & Carlson, C. A. (2001). Biogeochemistry of total organic carbon and nitrogen in the Sargasso Sea: Control by convective overturn. *Deep Sea Research Part II: Topical Studies in Oceanography*, *48*(8), 1649–1667. https://doi.org/10.1016/S0967-0645(00)00153-3

Honjo, S. (1980). Material fluxes and modes of sedimentation in the mesopelagic and bathypelagic zones. *Journal of Marine Research*.

Jónasdóttir, S. H. (2019). Fatty Acid Profiles and Production in Marine Phytoplankton. *Marine Drugs*, *17*(3), 151. https://doi.org/10.3390/md17030151

562 Karl, D. M., & Grabowski, E. (2017). The Importance of H in Particulate Organic Matter
563 Stoichiometry, Export and Energy Flow. *Frontiers in Microbiology*, *8*, 826.
564 https://doi.org/10.3389/fmicb.2017.00826

565 Keeling, R. E., Körtzinger, A., & Gruber, N. (2010). Ocean deoxygenation in a warming
566 world. *Annual Review of Marine Science*, *2*, 199–229.
567 https://doi.org/10.1146/annurev.marine.010908.163855

568 Klausmeier, C. A., Litchman, E., & Levin, S. A. (2004). Phytoplankton growth and
569 stoichiometry under multiple nutrient limitation. *Limnology and Oceanography*, *49*(4part2),
570 1463–1470. https://doi.org/10.4319/lo.2004.49.4_part_2.1463

571 Latasa, M., Cabello, A. M., Morán, X. A. G., Massana, R., & Scharek, R. (2017).
572 Distribution of phytoplankton groups within the deep chlorophyll maximum. *Limnology and*
573 *Oceanography*, *62*(2), 665–685. https://doi.org/10.1002/lno.10452

574 Laws, E. A. (1991). Photosynthetic quotients, new production and net community
575 production in the open ocean. *Deep Sea Research Part A. Oceanographic Research*
576 *Papers*, *38*(1), 143–167. https://doi.org/10.1016/0198-0149(91)90059-O

577 Lee, C., Wakeham, S., & Arnosti, C. (2004). Particulate Organic Matter in the Sea: The
578 Composition Conundrum. *Ambio*, *33*(8), 565–575.

579 Levin, L. A. (2018). Manifestation, Drivers, and Emergence of Open Ocean Deoxygenation.
580 *Annual Review of Marine Science*, *10*(1), 229–260. https://doi.org/10.1146/annurev-
581 marine-121916-063359

582 Liefer, J. D., Garg, A., Fyfe, M. H., Irwin, A. J., Benner, I., Brown, C. M., et al. (2019). The
583 Macromolecular Basis of Phytoplankton C:N:P Under Nitrogen Starvation. *Frontiers in*
584 *Microbiology*, *10*. https://www.frontiersin.org/articles/10.3389/fmicb.2019.00763

585 Liu, H., Wang, F., Liu, H., & Jing, H. (2022). Metabolic activity and community structure of
586 prokaryotes associated with particles in the twilight zone of the South China Sea. *Frontiers*
587 *in Microbiology*, *13*, 1056860. https://doi.org/10.3389/fmicb.2022.1056860

588 Lomas, M. W., Burke, A. L., Lomas, D. A., Bell, D. W., Shen, C., Dyhrman, S. T., &
589 Ammerman, J. W. (2010). Sargasso Sea phosphorus biogeochemistry: An important role

for dissolved organic phosphorus (DOP). *Biogeosciences*, *7*(2), 695–710. https://doi.org/10.5194/bg-7-695-2010

Lomas, M. W., & Moran, S. B. (2011). Evidence for aggregation and export of cyanobacteria and nano-eukaryotes from the Sargasso Sea euphotic zone. *Biogeosciences*, *8*(1), 203–216. https://doi.org/10.5194/bg-8-203-2011

Martin, J. H., Knauer, G. A., Karl, D. M., & Broenkow, W. W. (1987). VERTEX: Carbon cycling in the northeast Pacific. *Deep Sea Research Part A. Oceanographic Research Papers*, *34*(2), 267–285. https://doi.org/10.1016/0198-0149(87)90086-0

Moreno, A. R., Garcia, C. A., Larkin, A. A., Lee, J. A., Wang, W.-L., Moore, et al. (2020). Latitudinal gradient in the respiration quotient and the implications for ocean oxygen availability. *Proceedings of the National Academy of Sciences*, *117*(37), 22866–22872. https://doi.org/10.1073/pnas.2004986117

Moreno, A. R., Larkin, A. A., Lee, J. A., Gerace, S. D., Tarran, G. A., & Martiny, A. C. (2022). Regulation of the Respiration Quotient Across Ocean Basins. *AGU Advances*, *3*(5), e2022AV000679. https://doi.org/10.1029/2022AV000679

Olesen, M., & Lundsgaard, C. (1995). Seasonal sedimentation of autochthonous material from the euphotic zone of a coastal system. *Estuarine, Coastal and Shelf Science*, *41*(4), 475–490. https://doi.org/10.1016/0272-7714(95)90005-5

Ono, S., Ennyu, A., Najjar, R. G., & Bates, N. R. (2001). Shallow remineralization in the Sargasso Sea estimated from seasonal variations in oxygen, dissolved inorganic carbon and nitrate. *Deep Sea Research Part II: Topical Studies in Oceanography*, *48*(8), 1567–1582. https://doi.org/10.1016/S0967-0645(00)00154-5

Oschlies, A., Brandt, P., Stramma, L., & Schmidtko, S. (2018). Drivers and mechanisms of ocean deoxygenation. *Nature Geoscience*, *11*(7), Article 7. https://doi.org/10.1038/s41561-018-0152-2

Paulmier, A., Kriest, I., & Oschlies, A. (2009). Stoichiometries of remineralisation and denitrification in global biogeochemical ocean models. *Biogeosciences*, *6*(5), 923–935. https://doi.org/10.5194/bg-6-923-2009

Rayati, M., Rajabi Islami, H., & Shamsaie Mehrgan, M. (2020). Light Intensity Improves Growth, Lipid Productivity, and Fatty Acid Profile of Chlorococcum oleofaciens (Chlorophyceae) for Biodiesel Production. *BioEnergy Research*, *13*(4), 1235–1245. https://doi.org/10.1007/s12155-020-10144-5

Redfield, Alfred C. (1934). On the Proportions of Organic Derivatives in Sea Water and Their Relation to the Composition of Plankton. *James Johnstone Memorial Volume* (pp. 176-192). University Press of Liverpool.

Robinson, C. (2019). Microbial Respiration, the Engine of Ocean Deoxygenation. *Frontiers in Marine Science*, *5*. https://www.frontiersin.org/articles/10.3389/fmars.2018.00533

Sanderson, M, et al. (1997). Chapter 8. The Determination of Nitrite, Nitrate + Nitrite, Orthophosphate and Reactive Silicate in Sea Water Using Continuous Flow Analysis. *BATS Methods* (pp. 49-57). Bermuda Biological Station For Research, Inc.

Schmidtko, S., Stramma, L., & Visbeck, M. (2017). Decline in global oceanic oxygen content during the past five decades. *Nature*, *542*(7641), Article 7641. https://doi.org/10.1038/nature21399

Schneider, B., Karstensen, J., Oschlies, A., & Schlitzer, R. (2005). Model-based evaluation of methods to determine C:N and N:P regeneration ratios from dissolved nutrients. *Global Biogeochemical Cycles*, *19*(2). https://doi.org/10.1029/2004GB002256

Schneider, B., Schlitzer, R., Fischer, G., & Nöthig, E.-M. (2003). Depth-dependent elemental compositions of particulate organic matter (POM) in the ocean. *Global Biogeochemical Cycles*, *17*(2). https://doi.org/10.1029/2002GB001871

Shanks, A. L., & Trent, J. D. (1980). Marine snow: Sinking rates and potential role in vertical flux. *Deep Sea Research Part A. Oceanographic Research Papers*, *27*(2), 137–143. https://doi.org/10.1016/0198-0149(80)90092-8

Shepherd, J. G., Brewer, P. G., Oschlies, A., & Watson, A. J. (2017). Ocean ventilation and deoxygenation in a warming world: Introduction and overview. *Philosophical Transactions of the Royal Society A: Mathematical, Physical and Engineering Sciences*, *375*(2102), 20170240. https://doi.org/10.1098/rsta.2017.0240

Stoner, A., & Greening, H. (1984). Geographic variation in the macrofaunal associates of pelagic Sargassum and some biogeographic implications. *Marine Ecology Progress Series*, *20*, 185–192. https://doi.org/10.3354/meps020185

Stramma, L., Oschlies, A., & Schmidtko, S. (2012). Mismatch between observed and modeled trends in dissolved upper-ocean oxygen over the last 50 yr. *Biogeosciences*, *9*(10), 4045–4057. https://doi.org/10.5194/bg-9-4045-2012

Suárez, I., & Marañón, E. (2003). Photosynthate allocation in a temperate sea over an annual cycle: The relationship between protein synthesis and phytoplankton physiological state. *Journal of Sea Research*, *50*(4), 285–299. https://doi.org/10.1016/j.seares.2003.04.002

Takahashi, T., Broecker, W. S., & Langer, S. (1985). Redfield ratio based on chemical data from isopycnal surfaces. *Journal of Geophysical Research: Oceans*, *90*(C4), 6907–6924. https://doi.org/10.1029/JC090iC04p06907

Tanioka, T., Matsumoto, K., & Lomas, M. W. (2021). Drawdown of Atmospheric pCO2 Via Variable Particle Flux Stoichiometry in the Ocean Twilight Zone. *Geophysical Research Letters*, *48*(22), e2021GL094924. https://doi.org/10.1029/2021GL094924

Terzić, E., Lazzari, P., Organelli, E., Solidoro, C., Salon, S., D'Ortenzio, F., & Conan, P. (2019). Merging bio-optical data from Biogeochemical-Argo floats and models in marine biogeochemistry. *Biogeosciences*, *16*, 2527–2542. https://doi.org/10.5194/bg-16-2527-2019

Wang, W.-L., Moore, J. K., Martiny, A. C., & Primeau, F. W. (2019). Convergent estimates of marine nitrogen fixation. *Nature*, *566*(7743), Article 7743. https://doi.org/10.1038/s41586-019-0911-2